Stability of variable density rotating flows: Inviscid case and viscous effects in the limit of large Reynolds numbers

C. Jacques, B. Di Pierro ®,* F. Alizard ®, and M. Buffat
Univ Lyon, Université Claude Bernard Lyon I, Ecole Centrale de Lyon, INSA Lyon, CNRS, Laboratoire de Mécanique des Fluides et d'Acoustique, UMR 5509, 43 boulevard du 11 novembre 1918, F-69100 Villeurbanne, France

A. Cadiou ® and L. Le Penven ®
Univ Lyon, Ecole Centrale de Lyon, INSA Lyon, Université Claude Bernard Lyon I, CNRS, Laboratoire de Mécanique des Fluides et d'Acoustique, UMR 5509, 36 Avenue Guy de Collongue, F-69134 Ecully, France

Linear stability of solid body rotating flows with axisymmetric density variations is addressed analytically. Considering inviscid disturbances, a nontrivial dispersion relation is obtained and it is shown that the instability is of Rayleigh-Taylor type in cylindrical frame. The viscous correction is derived, in the limit of large Reynolds numbers and large azimuthal wave numbers, allowing the determination of the most unstable mode. Theoretical predictions are checked by comparing them to (spectrally accurate) computed eigenvalues and direct numerical simulations.

I. INTRODUCTION

Rotating and swirling flows of gas mixtures (i.e., variable density flows) are encountered in a wide variety of industrial and geophysical flows. Rotating injectors and hurricanes are two examples illustrating the special case of solid-body rotation [1]. Understanding the dynamics of these flows is not only of fundamental interest but is also relevant for the development of control and optimization strategies.

It is well known that solid body rotation of a homogeneous fluid is a marginally stable configuration of Euler's equations [2,3], while viscosity has only a stabilizing influence. Hence, the so-called inertial waves have been experimentally observed only when the excitation source is sustained [4]. Considering three dimensional disturbances of a two-dimensional axisymetric basic configuration, the flow exhibits an instability if the Rayleigh-discriminant $\Phi = 2V(dV/dr + V/r)/r$ is negative somewhere in the flow [5] (r being the distance from rotation center and $V(r)$ the azimuthal velocity).

If density variations within the fluid are considered, an equivalent to the Brünt-Vaïssalla frequency G is usually defined by $G^2 = -(\Omega^2 r/\rho)d\rho/dr$ (ρ being the density and $\Omega = V/r$). Leibovich [6] and Howard [7] have shown independently that the flow is stable to axisymmetric disturbances if $G^2 < \Phi$, for both incompressible and compressible flows. For rotating flows with axial jet, Leibovich and Stewartson [5] have been able to theoretically derive the discrete spectrum of the instability near the point where the Doppler frequency $kW + m\Omega - \omega$ admits an extremum

---

*Corresponding author: bastien.di-pierro@univ-lyon1.fr

(ω, k, m, W being the pulsation, axial wavenumber, azimuthal wavenumber, and axial velocity, respectively). Subsequently, Eckhoff [8] derived a sufficient condition for instability using a WKB expansion. Those results have been extended by Leblanc and Le Duc [9], who established a link between the eigenfrequencies of [8] and [5]. Di Pierro and Abid [10] have proposed an asymptotic expression for the eigenfrequency associated with rotating flow with axial jet, assuming large wavenumbers.

Along with that, Gans [11] has shown that the flow is unstable with respect to any nonaxisymmetric two-dimensional disturbances if G^2 is slightly positive. Additionally, considering an equivalent configuration, Sipp *et al.* [12] have shown through numerical experiments that $G^2 > 0$ is a necessary condition for such an instability. The authors argued that the underlying mechanism was associated with a Rayleigh-Taylor instability.

More recently, Scase and Hill [13] investigated both theoretically and numerically the effect of rotation on confined two liquid layers, with different density and viscosity, that form concentric cylinders. Their axis of rotation is confused with central axes of these cylinders. The authors have also discussed the effect of rotation of both miscible and immiscible fluids. For all flow cases, the equilibrium state is associated with the two-layers initially separated by a sharp interface. An Orr-Sommerfeld-like equation is derived which successfully reproduces direct numerical simulations as long as the linear approximation is still valid. Especially, they have shown that the system may be unstable when the inner fluid is denser than the outer one driven by the centrifugal force. The instability takes the form of mushroom like perturbations in the nonlinear regime as observed in the Rayleigh-Taylor configuration. Scase and Sengupta [14] extended these results to a three dimensional configuration. They showed that the disturbances growth is essentially driven by geometrical parameters in the absence of surface tension: domain aspect ratio and initial position of the interface. While the above findings provide a good understanding of the amplification of Rayleigh-Taylor-like instability in a centrifugally driven configuration, it does not discuss the case of initial gas mixtures and spatially extended configuration in the radial direction. Finally, an equivalent configuration of a cylindrical biphasic flow with uniform radial acceleration has been studied by Zeng *et al.* [15]. They observed both two- and three-dimensional disturbances and, particularly, they showed that the growth rate of the two-dimensional mode varies as $\nu^{1/3}$ (ν the kinematic viscosity), while the three dimensional regime is very dependent of the viscosity ratio.

The purpose of this paper is then to investigate certain aspects of Rayleigh-Taylor instability in rotating flows and to extend previously mentioned studies. The studied configuration is a steady, solid-body rotation and incompressible flow in the presence of a radial smooth density gradient. Two results are obtained: (i) an analytical dispersion relation without any asymptotic consideration in the inviscid case and (ii) a viscous correction in the limit of large Reynolds numbers. The present study allows an extension of some conclusions in [10], which are limited to a large wavenumber and inviscid analysis. This paper also extends the study of [12] which numerically deals with the stability of inviscid Gaussian vortex with heavy cores. The present study corresponds to the case of nonaxial flow $W(r) = 0$ of [10] and small density core length $b \to 0$ of [12]. In particular, it is shown that a sufficient condition for instability is $G^2 > 0$ somewhere in the flow for any density ratio, and that the viscous correction has a purely stabilizing effect, allowing the determination of the most unstable mode. A very good agreement between the analytical dispersion relation and (linear/nonlinear) numerical simulations is obtained.

The paper is organized as follows. In Sec. II, the problem formulation is stated with mathematical and numerical considerations. Section III establishes the inviscid dispersion relation, and Sec. IV deals with the viscous correction. Both are validated by comparison with computed eigenvalues in these two sections. Finally, those results are compared with direct numerical simulations in Sec. V, and the last section provides some physical discussion and concluding remarks.
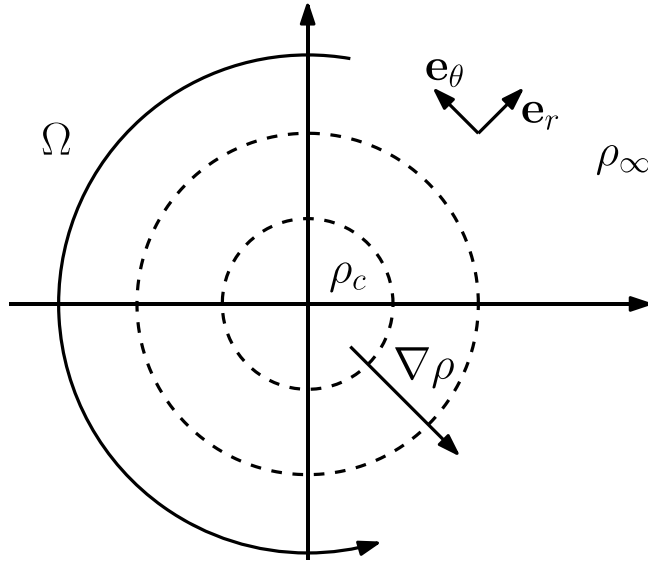
FIG. 1. Sketch of the basic flow.

II. PROBLEM FORMULATION

A. Governing equations

The incompressible, variable-density Navier-Stokes equations are considered, neglecting molecular diffusion [16]:

$$\frac{\partial \mathbf{u}}{\partial t} = -(\mathbf{u}\,\nabla)\mathbf{u} - \frac{1}{\rho}\nabla P + \frac{\mu}{\rho}\Delta\mathbf{u}, \tag{1}$$

$$\frac{\partial \rho}{\partial t} = -\mathbf{u}\,\nabla\rho, \tag{2}$$

$$\nabla\,\mathbf{u} = 0, \tag{3}$$

with $\mathbf{u}$ the vector velocity field, ρ the density, and P the pressure. The dynamic viscosity μ is assumed to be constant, which is representative of gaseous or liquid mixtures, and the surface tension is neglected. We investigate a steady solid-body rotation base flow with rotation rate Ω and an axisymmetric density profile, as seen in Fig. 1. By introducing R, the density core length, as the length scale and Ω^{-1} as the time scale, one can define the Reynolds number $Re = \rho_\infty \Omega R^2/\mu$ where ρ_∞ is the density far from the rotating center. The velocity, pressure and density fields of the base flow are expressed in polar coordinates (r, θ) as $\mathbf{U_0}(r) = \Omega r \mathbf{e}_\theta$, $P_0(r)$, and $\rho_0(r)$, respectively. We consider two-dimensional disturbances of the form

$$(u_r(\mathbf{x}, t),\ u_\theta(\mathbf{x}, t),\ \rho(\mathbf{x}, t),\ P(\mathbf{x}, t))^T = (u(r),\ v(r),\ \rho(r),\ p(r))^T \exp(i(m\theta - \omega t)), \tag{4}$$

with m the azimuthal wavenumber and ω the unknown complex pulsation. Linearization of Eqs. (1), (2), and (3) leads to the following eigensystem:

$$i\left(m\Omega - \omega + i\frac{\mathcal{L}}{Re\rho_0}\right)u - 2\left(\Omega - \frac{im}{Re\rho_0 r^2}\right)v + \frac{1}{\rho_0}\frac{dP}{dr} - \frac{\Omega^2 r}{\rho_0}\rho = 0,$$

$$2\left(\Omega - \frac{im}{Re\rho_0 r^2}\right)u + i\left(m\Omega - \omega + i\frac{\mathcal{L}}{Re\rho_0}\right)v + \frac{im}{r\rho_0}P = 0,$$

$$i(m\Omega - \omega)\rho + u\frac{d\rho_0}{dr} = 0,$$

$$\frac{1}{r}\frac{dru}{dr} + \frac{im}{r}v = 0, \qquad (5)$$

with $\mathcal{L} = \frac{d^2}{dr^2} + \frac{1}{r}\frac{d}{dr} - \frac{m^2+1}{r^2}$.

B. Numerical resolution

The eigenvalues and eigenfunctions (u, v, ρ, p) are computed with spectral accuracy by using Chebyshev polynomial expansions. The infinite domain $r \in [-\infty, \infty]$ is mapped to the interval $\gamma \in [-1, 1]$ containing the Gauss-Lobato points $(\gamma_i = \cos(i\pi/(N-1)),\ i = 0, \ldots, N-1)$ using the transformation $r = \tan(\pi\gamma/2)$. This transformation avoids the expression of a boundary condition at $r = 0$, which depends on the disturbance symmetry. The number of modes N is even such that the singular point $r = 0$ is avoided. In the following, the radial derivative operators of order n will be denoted by D_r^n [17].

Since the equation associated with the pressure is independent of ω, system (5) is numerically illconditioned. This leads to the computation of nonphysical oscillating modes [17]. To avoid the occurrence of these spurious modes when solving the eigensystem, the pressure is eliminated from (5) by taking the divergence of the momentum equations and using the inverse of an elliptic operator:

$$\mathbb{D} = \left[\frac{m^2}{r^2\rho_0} - \left(D_r + \frac{1}{r}\right)\frac{1}{\rho_0}D_r\right]^{-1}. \qquad (6)$$

Now, the eigenvalue problem can be recast as:

$$\mathcal{A}\begin{pmatrix} u \\ v \\ \rho \end{pmatrix} = i\omega\begin{pmatrix} u \\ v \\ \rho \end{pmatrix}, \qquad (7)$$

with

$$\mathcal{A} = \begin{bmatrix} im\Omega - \frac{1}{Re\rho_0}\mathbb{L} + \frac{1}{\rho_0}D_r\mathbb{D}C_u & -2\left(\Omega - \frac{im}{Re\rho_0 r^2}\right) + \frac{1}{\rho_0}D_r\mathbb{D}C_v & \frac{-\Omega^2 r}{\rho_0} + \frac{1}{\rho_0}D_r\mathbb{D}C_\rho \\ 2\left(\Omega - \frac{im}{Re\rho_0 r^2}\right) + \frac{im}{\rho_0 r}\mathbb{D}C_u & im\Omega - \frac{1}{Re\rho_0}\mathbb{L} + \frac{im}{\rho_0 r}\mathbb{D}C_v & \frac{im}{\rho_0 r}\mathbb{D}C_\rho \\ \frac{d\rho_0}{dr} & 0 & im\Omega \end{bmatrix},$$

$$\begin{cases} C_u = \left(D_r + \frac{1}{r}\right)\left(im\Omega - \frac{1}{Re\rho_0}\mathbb{L}\right) + 2\frac{im}{r}\left(\Omega - \frac{im}{r^2 Re\rho_0}\right) \\ C_v = -2\left(D_r + \frac{1}{r}\right)\left(\Omega - \frac{im}{r^2 Re\rho_0}\right) + \frac{im}{r}\left(im\Omega - \frac{1}{Re\rho_0}\mathbb{L}\right) \\ C_\rho = -\left(D_r + \frac{1}{r}\right)\frac{\Omega^2 r}{\rho_0}, \end{cases}$$

and $\mathbb{L} = D_r^2 + (1/r)D_r - (m^2 + 1)/r^2$. In addition to eliminating spurious modes, elimination of the pressure improves operator conditioning and accelerates the computation of eigenvalues. The last eigensystem (7) is solved using LAPACK routines.

For numerical validation, the following basic density profile is used:

$$\rho_0(r) = 1 + \frac{s-1}{2}\left(1 - \tanh\left(\frac{r-1}{e}\right)\right), \tag{8}$$

which mimics heavy (or light) vortex core with smooth density variations; e being the variation length of density profile and s being the density ratio between the rotating center and the far field.

III. INVISCID INSTABILITY

In the limit of an infinite Reynolds number, the system (5) can be rewritten as a single equation of the variable $\phi = ru$, as

$$\frac{d^2\phi}{dr^2} + \frac{1}{\rho_0 r}\frac{d\rho_0 r}{dr}\frac{d\phi}{dr} - \left[\frac{2m\Omega}{r\rho_0\Sigma}\frac{d\rho_0}{dr} + \frac{m^2}{r^2}\left(1 + \frac{G^2}{\Sigma^2}\right)\right]\phi = 0, \tag{9}$$

with

$$G^2 = -\frac{\Omega^2 r}{\rho_0}\frac{d\rho_0}{dr}, \quad \Sigma = m\Omega - \omega. \tag{10}$$

Introducing $\psi = \sqrt{r\rho_0}\phi$, Eq. (9) becomes

$$\frac{d^2\psi}{dr^2} + \left[\zeta - \frac{2m\Omega}{r\rho_0\Sigma}\frac{d\rho_0}{dr} - \frac{m^2}{r^2}\left(1 + \frac{G^2}{\Sigma^2}\right)\right]\psi = 0, \tag{11}$$

with

$$\zeta = \left[\frac{1}{2\rho_0 r}\frac{d\rho_0 r}{dr}\right]^2 - \frac{1}{2\rho_0 r}\frac{d^2\rho_0 r}{dr^2}. \tag{12}$$

From (11), we assume that the unstable dynamics occurs at the location r^*, such that $G^2(r^*)$ is a local extremum. Introducing, $\tilde{r} = r - r^*$ and $\tilde{\psi}(\tilde{r}) = \psi(r)$, a second order Taylor expansion of (11) gives

$$\frac{d^2\tilde{\psi}}{d\tilde{r}^2} + \Theta(\tilde{r})\tilde{\psi} = 0, \tag{13}$$

with

$$\Theta(\tilde{r}) = \zeta(r^*) - \frac{\chi(r^*)}{r^{*2}} + \left(\frac{d\zeta}{dr}(r^*) + \frac{2\chi(r^*)}{r^{*3}}\right)\tilde{r} + \left(\frac{d^2\zeta}{dr^2}(r^*) - \frac{1}{r^{*2}}\frac{d^2\chi}{dr^2}(r^*) - \frac{6\chi(r^*)}{r^{*4}}\right)\frac{\tilde{r}^2}{2},$$

$$\chi(r) = 2m\frac{G^2}{\Omega\Sigma} + m^2\left(1 + \frac{G^2}{\Sigma^2}\right). \tag{14}$$

Equation (13) is a parabolic cylinder equation. Assuming that ψ vanishes far from r^*, Eq. (13) admits solutions in the form of Weber-Hermite polynomials $\tilde{\psi}(\tilde{r}) = H_n(\alpha\tilde{r} + \beta)$ with

$$\alpha = \sqrt{2}\left(3\frac{\chi(r^*)}{r^{*4}} + \frac{1}{2r^{*2}}\frac{d^2\chi}{dr^2}(r^*) - \frac{1}{2}\frac{d^2\zeta}{dr^2}(r^*)\right)^{1/4}, \quad \beta = \frac{2}{\alpha^3}\left(\frac{d\zeta}{dr}(r^*) + \frac{2\chi(r^*)}{r^{*3}}\right), \tag{15}$$

if and only if

$$-\frac{1}{\alpha^2}\left(\frac{\chi(r^*)}{r^{*2}} - \zeta(r^*) + \frac{\left(\frac{d\zeta}{dr}(r^*) + \frac{2\chi(r^*)}{r^{*3}}\right)^2}{2\frac{d^2\zeta}{dr^2}(r^*) - 2\frac{1}{r^{*2}}\frac{d^2\chi}{dr^2}(r^*) - \frac{12\chi(r^*)}{r^{*3}}}\right) = n + \frac{1}{2}, \tag{16}$$

where n is an integer. This inviscid dispersion relation corresponds to the case studied numerically in [12] for small density distribution widths (defined as "b" in their paper). Note that it is not based
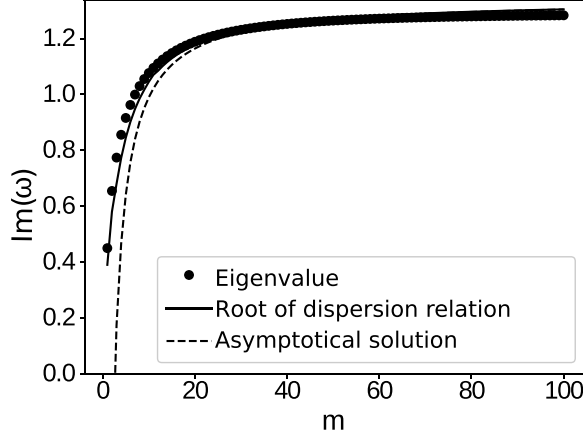
FIG. 2. Inviscid dispersion relation $Im(\omega)$ versus azimuthal wavenumber m for density ratio $s = 2$ and mass thickness $e = 0.2$ [Dotted: eigenvalue of system (7), line: root of dispersion relation (16), dashed: Asymptotical solution (17)].

on the assumption of a weakly varying base flow [10] or large wavenumbers. In the limit of large azimuthal wavenumbers, the following growth rate is obtained by expansion of (16) with respect to m:

$$\omega_n = m\Omega + \frac{G^2}{m\Omega} + i\left(\sqrt{G^2(r^*)} + \frac{n + \frac{1}{2}}{m}\sqrt{-\frac{r^{*2}}{2}\frac{d^2G^2}{dr^2}(r^*)}\right). \tag{17}$$

Here, the expression (17) is identical to the one obtained in [10], except for the correction $G^2/m\Omega$ to the real part. Equation (16) has no explicit solution, and is numerically solved using the Muller's root finding algorithm [18].

Figure 2 compares the dispersion relation obtained using the full system (7) to the solution of (16) and the asymptotic expression (17). A very good agreement is found: the solutions of system (7) and equation (16) are almost undistinguishable, and the relative error is less than 10% if $m \geqslant 6$ when comparing the solutions of (7) and (17).

IV. ASYMPTOTIC VISCOUS INSTABILITY

The viscous case is considered here in the limit of large Reynolds numbers as well as large wave numbers, such that $1 \ll m^2 \ll Re$. Hence, $m^2 Re^{-1}$ is treated as a small parameter. In this limit, the viscous operator behaves to leading order as

$$\frac{1}{Re}\mathcal{L} \approx \frac{-m^2}{r^2 Re}. \tag{18}$$

The differential system (5) can then be rewritten as a second order differential equation:

$$\frac{d^2\phi}{dr^2} + \left[\frac{1}{\rho_0 r}\frac{d\rho_0 r}{dr} + \frac{1}{\Sigma + i\mathcal{N}}\frac{d\mathcal{N}}{dr}\right]\frac{d\phi}{dr}$$
$$- \left[\frac{2m(\Omega - i\mathcal{M})}{r\rho_0(\Sigma + i\mathcal{N})}\frac{d\rho_0}{dr} + \frac{m^2}{r^2}\left(1 + \frac{G^2}{\Sigma(\Sigma + i\mathcal{N})}\right) - \frac{2im}{r}\frac{1}{\Sigma + i\mathcal{N}}\frac{d\mathcal{M}}{dr}\right]\phi = 0, \quad (19)$$

with

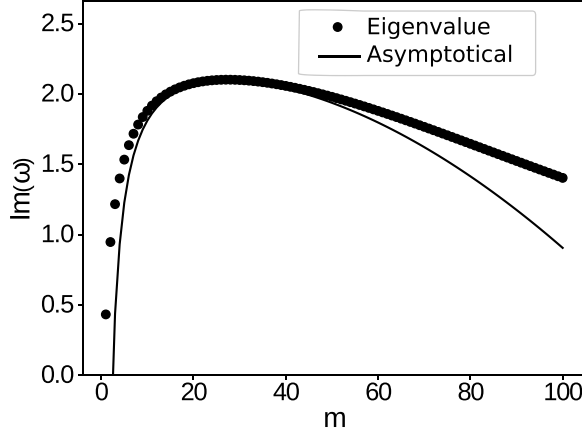$$\mathcal{N} = \frac{-m^2}{r^2 Re}, \quad \mathcal{M} = \frac{m}{r^2 Re}. \tag{20}$$

FIG. 3. Growth rate $Im(\omega)$ versus azimuthal wavenumber m for $s = 10$, $e = 0.2$, and $Re = 1000$ [Dotted: eigenvalue of system (7), line: Asymptotical solution (22)].

Proceeding in the same way as in the previous section, one gets to leading order in m and m^2/Re:

$$\frac{d^2\psi}{dr^2} - \left[\frac{2mG^2}{r^2\Omega(\Sigma + i\mathcal{N})} + \frac{m^2}{r^2}\left(1 + \frac{G^2}{\Sigma(\Sigma + i\mathcal{N})}\right)\right]\psi = 0, \qquad (21)$$

with $\psi = \sqrt{\rho_0 r(\Sigma + i\mathcal{N})}\phi$. Here again, a parabolic cylinder equation is found, whose solutions are Weber-Hermite polynomials associated with the following dispersion relation:

$$\omega_n = m\Omega + \frac{G^2(r^*)}{\Omega m} + i\left(\sqrt{G^2(r^*)} - \frac{n + 1/2}{m}\sqrt{-\frac{r^{*2}}{2}\frac{d^2G^2}{dr^2}(r^*)} - \frac{m^2}{2Re\rho_0(r^*)r^{*2}}\right). \qquad (22)$$

Figure 3 shows the imaginary part of the eigenfrequencies obtained numerically in comparison with the asymptotic solution (the real parts being indistinguishable). It appears that Eq. (22) is a good approximation when $12 \leqslant m \leqslant 50$ (the error is less than 2.5%); i.e., in the limit of large m and $m^2 Re^{-1} \lesssim O(1)$. Moreover, one can see that the maximum of the dispersion curve (see Fig. 3) is correctly represented by this last approximation. This allows the identification of the most unstable mode as well as the corresponding azimuthal wavenumber:

$$\omega_{n,\max} = m\Omega + \frac{G^2(r^*)}{\Omega m} + i\sqrt{G^2} - \frac{3i}{2}\frac{\left((n + \frac{1}{2})\sqrt{-\frac{r^{*2}}{2}\frac{d^2G^2}{dr^2}(r^*)}\right)^{\frac{2}{3}}}{(r^{*2}\rho_0(r^*)Re)^{\frac{1}{3}}}, \qquad (23)$$

$$m_{\max} = \left(\left(n + \frac{1}{2}\right)Re\rho_0(r^*)r^{*2}\right)^{\frac{1}{3}}\left(-\frac{r^{*2}}{2}\frac{d^2G^2(r^*)}{dr^2}\right)^{\frac{1}{6}}. \qquad (24)$$

A comparison between these approximations and numerical solutions is shown in Fig. 4. Very good agreement is found for the most amplified mode $\omega_{n,\max}$ as well as for the selected azimuthal mode $m_{n,\max}$.

V. NONLINEAR INSTABILITY

To analyze the instability dynamics towards the non linear stage, the variable density Navier-Stokes equations (1), (2), and (3) are solved numerically using the method presented in [19]. Here is a brief review. The spatial discretization is based on a two-dimensional Fourier expansion, with periodic boundary conditions. Time integration is performed using a second order Runge-Kutta scheme,
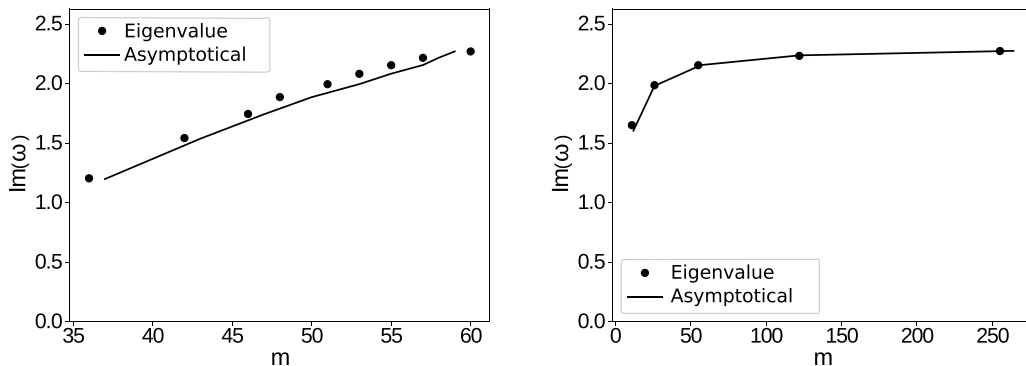
FIG. 4. Numerical and asymptotical growth rate $Im(\omega_{n,\max})$ versus $m_{\max}$ for the most unstable mode for $e = 0.2$. Left: $Re = 10^4$ and $s = 2,\ 3,\ 4,\ 5,\ 6,\ 7,\ 8,\ 9,\ 10$. Right: $s = 8$ and $Re = 10^2,\ 10^3,\ 10^4,\ 10^5,\ 10^6$ [Dotted: eigenvalue of system (7), line: Asymptotical solution (23) and (24)].

while the pressure is computed using a fixed point method to ensure the incompressibility constraint. The time step is chosen as 10^{-2} in order to satisfy stability criterion, and the computational domain is a square of size $6\pi \times 6\pi$ discretized with 512×512 grid points. The initial density profile (8) is used. The velocity initial condition is a Lamb-Oseen-like vortex: $\Delta(U_\theta \mathbf{e}_\theta) = -\nabla \times (\Omega_{LO}(r)\mathbf{e}_z)$, with $\Omega_{LO}(r) = \Omega \exp(-r^2/a^2)$ the vorticity and $a = 5$. The latter velocity field is then compatible with periodic boundary conditions [20]. A plot of the initial distribution is shown in Fig. 5 (top left). Note that the dynamics within the vortex core ($r \lesssim 0.3a$) is close to a solid body rotation. In the case of constant density, the Lamb-Oseen vortex does not satisfy the instability conditions of Leibovich & Stewartson [5]. Its linear stability has been proven numerically by [21]. Finally, the flow is initially disturbed with a random noise of amplitude $O(10^{-3})$.

The disturbance amplitudes A_m of each mode m are extracted from the Fourier expansion $\hat{\rho}_m(r, t)$ of the density field $\rho(r, \theta, t)$ interpolated from the Cartesian grid (x, y), and are defined as

$$A_m(t) = \sqrt{\int_0^R |\hat{\rho}_m(r, t)|^2 r\, dr}. \tag{25}$$

Figure 5 shows a contour plot of the density field at times $t \approx 3.7, 5.5,$ and 7.4 for $Re = 1000$ and $s = 2$. At the earliest times, many azimuthal modes are growing (Fig. 5, top right), while the azimuthal mode $m \approx 17$ emerges a little later on (Fig. 5, bottom left). This last mode is the most unstable, which is predicted by the asymptotic expression $m_{\max}$ (24).

Figure 6 shows the amplitude of the $m = 17$ mode versus time and the asymptotic prediction $\exp(-i\omega_{n,\max}t)$ [see Eqs. (23) and (24)]; $Im(\omega_{n,\max}) \approx 1.04$ with the considered parameters for this mode. After a transient time, one can see that the exponential growth is well represented by the asymptotic theory. For $t \approx 7$, Fig. 5 (bottom right) shows that the instability reaches a nonlinear stage where modal interactions can no longer be neglected. The study of these nonlinear interactions is left for future work. A last simulation where $e/R = O(1)$ has been performed, with the basic flow

$$\rho_0(r) = 1 + (s - 1)\exp(-r^2). \tag{26}$$

The comparison between direct numerical simulation and prediction of (23) is shown in Fig. 7. Once again, a very good agreement is found.

VI. DISCUSSION AND CONCLUSION

The paper presents a linear temporal stability analysis of an axisymmetric, variable-density, uniformly rotating flow evolving under the incompressibility constraint. The problem solutions are
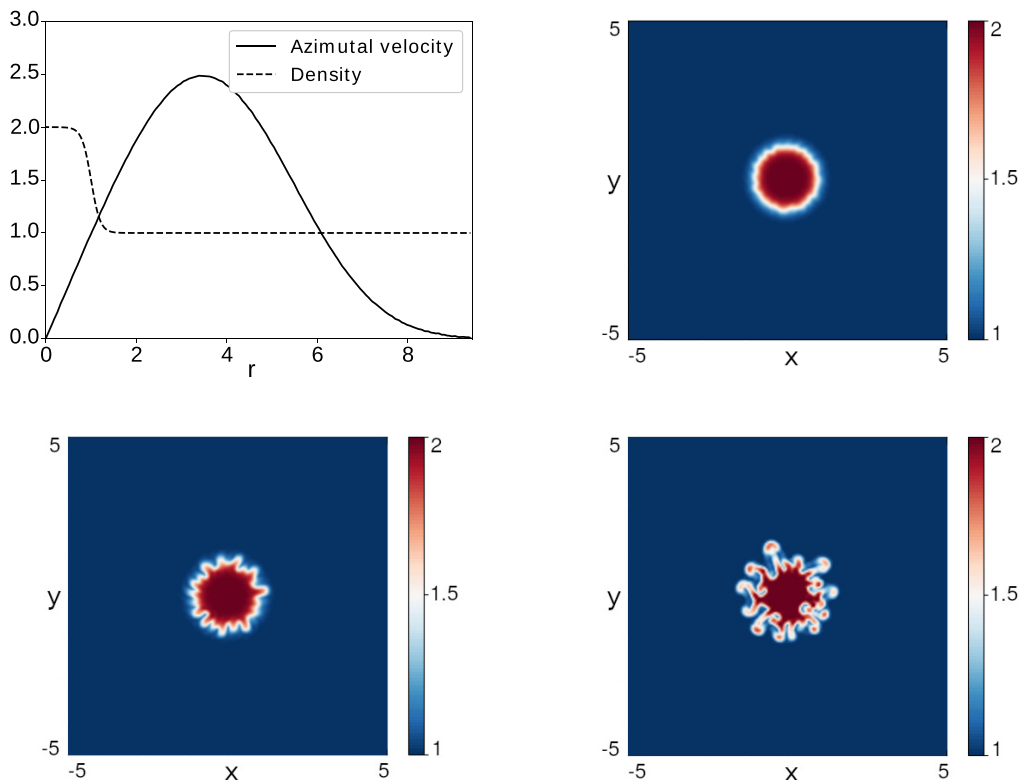
FIG. 5. Direct numerical simulation of the variable density rotating flow with $s = 2$ and $Re = 1000$. Initial radial distribution (top left), Iso-contours of density field at time $t \approx 3.7$ (top right), $t \approx 5.5$ (bottom left), and $t \approx 7.4$ (bottom right). x and y here are the Cartesian coordinates.

validated by comparison to spectrally accurate numerical methods. In the inviscid case, which is considered first, the problem is governed by a second order differential equation. It is shown that the instability dynamics is characterized by an analog to the Brünt-Vaïssalla frequency $G(r)$ [with $G^2(r) = (-\Omega^2 r / \rho_0) d\rho_0 / dr$]. It is also shown that disturbances reach a maximum near the location where $G^2(r)$ admits an extremum. A nontrivial dispersion relation is obtained. However, in the limit of large azimuthal wavenumbers, an approximation of eigenfrequency can be analytically obtained. It can be seen that an instability can occur if and only if $G^2 > 0$ (i.e., if $d\rho_0 / dr < 0$). In that sense, it completes results given by Scase and Hill [13] restricted to the sharp initial density profile case and confined within a given radial distance from the rotating center. One deduces that the instability is triggered when the local centrifugal acceleration ($\mathbf{a_c} = \Omega^2 r \mathbf{e_r}$) and the reduced density gradient [$\bar{\nabla}\rho = (\nabla\rho_0)/\rho_0$] are in opposite directions. This shows that the resulting instability is a cylindrical Rayleigh-Taylor one, the disturbance growth rate being proportional to the maximum of $\sqrt{-\mathbf{a_c} \bar{\nabla}\rho}$. This is very similar to the classical planar Rayleigh-Taylor growth rate $\sqrt{gkA_t}$ (g, k, and A_t being the gravitational acceleration, the wavenumber, and the Atwood number, respectively). When comparing the expression of the eigenfrequencies at large m for solid-body rotation to the asymptotic result of [10] obtained assuming weakly-varying velocity profiles, it appears that the instability growth rates are the same up to order $1/m$. The only difference being that a change is observed in the the real frequency of order $1/m$. In the inviscid case, all modes are unstable and the instability growth rate is an increasing function of the azimuthal wavenumber approaching the asymptotic value $\sqrt{G^2}$ for large m. Hence, no mode selection is observed. To correctly represent
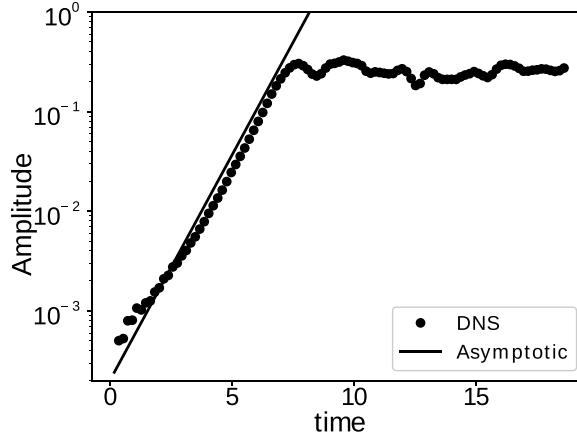
FIG. 6. Amplitude of the azimuthal mode $m = 17$ versus time, for $Re = 1000$ and $s = 2$ and the asymptotic prediction (23) and (24).

the mode selection, viscous effects have been studied in the limit of large Reynolds numbers as well as large m. The resulting dynamics equation is very similar to the inviscid one and viscosity appears as a purely stabilizing effect. Indeed, the real frequency is not affected by the viscous drag while the growth rate varies as $-m^2/(\rho_0 Re)$. Once again, this is remarkably similar to the planar Rayleigh-Taylor viscous correction proportional to $-k^2/(\rho_m Re)$ (ρ_m being an average density). Thus, the resulting instability exhibits competitive mechanisms between the inviscid Rayleigh-Taylor instability and to viscous damping. The most unstable mode has a growth rate varying as $Re^{-1/3}$, while the corresponding azimuthal wavenumber grows as $Re^{1/3}$. The latter scaling is very similar to the planar Rayleigh-Taylor instability for which the growth rate varies as $Re^{-1/3}$, while the corresponding longitudinal wavenumber grows as $Re^{2/3}$.

Considering three-dimensional disturbances for the same base flow (i.e., a columnar vortex), one notes that the dynamics equation remains the same when considering the modified wavenumber $l^2 = m^2 + k^2 r^2$, where k is the axial wavenumber. In particular, in the limit of large wavenumbers $l \to \infty$ and large Reynolds numbers, Eq. (19) remains invariant by substituting m with l. Hence, the same instability characteristics are obtained. Such three-dimensional disturbances are *helical* Rayleigh-Taylor instabilities. Such disturbances have been observed by Zeng *et al.* [15] for
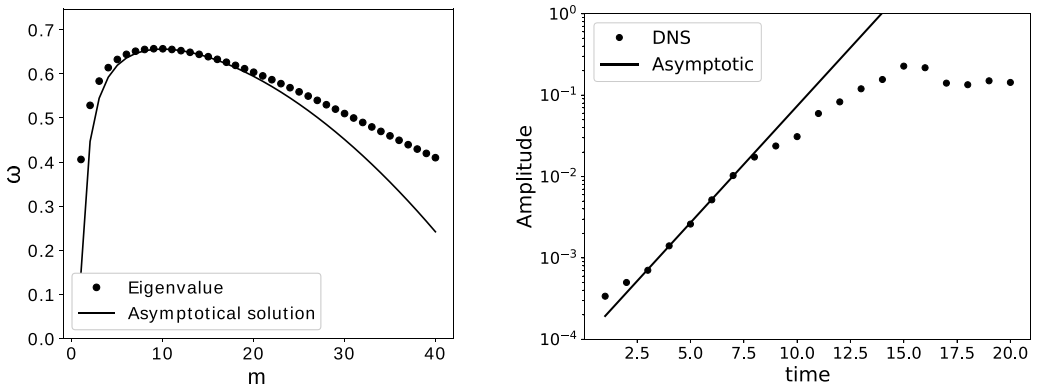

FIG. 7. Left: dispersion relation of base flow (26). Right: Amplitude of the azimuthal mode $m = 10$ versus time, for $Re = 1000$ and $s = 2$ and the asymptotic prediction (23) and (24), for base flow (26).

biphasic radially accelerated flows. Finally, these results have been validated using nonlinear direct numerical simulations where the instability is triggered by superimposing random noise of small amplitude onto the base flow. The most unstable mode observed in these simulations is in very good agreement with asymptotic theory. In the later times of the simulation, while nonlinearities appear, a strong modal interaction leads to the formation of mushroom-shaped disturbances, which are characteristics of a Rayleigh-Taylor instability. The resulting flow pattern is very similar to the one observed by Scase and Hill [13] in confined configuration.

ACKNOWLEDGMENT

---

[1] J. L. Lumley, *Engines: An Introduction* (Cambridge University Press, Cambridge, 1999).

[2] L. D. Landau and E. Lifchitz, *Course of Theoretical Physics, Fluid Mechanics* (Pergamon Press, 1987), Vol. 6.

[3] W. Thompson (Kelvin), *Hydrodynamics and General Dynamics, Mathematical and Physical Papers* (Cambridge University Press, Cambridge, 1910), Vol. IV.

[4] A. D. McEwan, Inertial oscillations in a rotating fluid cylinder, J. Fluid Mech. **40**, 603 (1970).

[5] S. Leibovich and K. Stewartson, A sufficient condition for the instability of columnar vortices, J. Fluid Mech. **126**, 335 (1983).

[6] S. Leibovich, Stability of density stratified rotating flows, AIAA J. **7**, 177 (1969).

[7] L. N. Howard, On the stability of compressible swirling flow, Stud. Appl. Math. **52**, 39 (1973).

[8] K. S. Eckhoff, A note on the instability of columnar vortices, J. Fluid Mech. **145**, 417 (1984).

[9] S. Leblanc and A. Le Duc, The unstable spectrum of swirling gas flows, J. Fluid Mech. **537**, 433 (2005).

[10] B. Di Pierro and M. Abid, Instabilities of variable-density swirling flows, Phys. Rev. E **82**, 046312 (2010).

[11] R. F. Gans, On the stability of shear flow in a rotating gas, J. Fluid Mech. **68**, 403 (1975).

[12] D. Sipp, D. Fabre, S. Michelin, and L. Jacquin, Stability of a vortex with a heavy core, J. Fluid Mech. **526**, 67 (2005).

[13] M. M. Scase and R. J. A. Hill, Centrifugally forced Rayleigh–Taylor instability, J. Fluid Mech. **852**, 543 (2018).

[14] M. M. Scase and S. Sengupta, Cylindrical rotating Rayleigh–Taylor instability, J. Fluid Mech. **907**, A33 (2021).

[15] R. H. Zeng, J. J. Tao, and Y. B. Sun, Three-dimensional viscous Rayleigh–Taylor instability at the cylindrical interface, Phys. Rev. E **102**, 023112 (2020).

[16] F. Guillén-González, P. Damázio, and M. A. Rojas-Medar, Approximation by an iterative method for regular solutions for incompressible fluids with mass diffusion, J. Math. Anal. Appl. **326**, 468 (2007).

[17] R. Peyret, *Spectral Methods for Incompressible Viscous Flow* (Springer Science & Business Media, 2013), Vol. 148.

[18] M. Lang and B.-C. Frenzel, Polynomial root finding, IEEE Signal Process. Lett. **1**, 141 (1994).

[19] B. Di Pierro and M. Abid, A projection method for the spectral solution of non-homogeneous and incompressible Navier-Stokes equations, Int. J. Numer. Methods Fluids **71**, 1029 (2013).

[20] B. Di Pierro and M. Abid, Rayleigh–Taylor instability in variable density swirling flows, Eur. Phys. J. B **85**, 1 (2012).

[21] D. Fabre, D. Sipp, and L. Jacquin, Kelvin waves and the singular modes of the lamb-oseen vortex, J. Fluid Mech. **551**, 235 (2006).